# Subject-Independent Continuous Estimation of sEMG-Based Joint Angles Using Both Multisource Domain Adaptation and BP Neural Network

He Li, *Student Member, IEEE*, Shuxiang Guo, *Fellow, IEEE*,
Hanze Wang, *Student Member, IEEE*, and Dongdong Bu, *Student Member, IEEE*

***Abstract*— Continuous angle estimation from surface electromyography (sEMG) is crucial for robot-assisted upper limb rehabilitation. The sEMG-based control provides an optimal way to achieve harmonic interactions between subjects and upper limb rehabilitation exoskeletons. Also, for upper limb exoskeleton systems with sEMG as the control signal, accurate identification of elbow angles from sEMG is essential. However, sEMG signals have a subject-specific nature, causing the estimation model with sEMG signals as input to have poor generalization across multiple subjects. Aiming at the above problem of intersubject variability on sEMG, multisource domain adaptation (MDA) is combined into the estimation of continuous joint movements to obtain subject-invariant features of sEMG. Also, the feature distribution of the training set and test set is evaluated using the kernel density estimation (KDE) method. Furthermore, the subject-invariant features obtained through MDA are the input of the backpropagation neural network (BPNN). Different evaluation indicators and the statistical method are used to compare the estimation results between original features and subject-invariant features, which proves the better generalization ability of the model based on subject-invariant features. Also, the estimation angle error calculated by using subject-invariant features as the input of BPNN is controlled within 10°, which shows the effectiveness of the combination of MDA and shallow neural network for the accurate subject-independent estimation of elbow joint continuous movements.**

***Index Terms*— BP neural network (BPNN), continuous angle estimation, intersubject variability, multisource domain adaptation (MDA), surface electromyography (sEMG).**

## I. Introduction

ACCORDING to the World Stroke Organization, stroke is the second-leading cause of death and the third-leading cause of death and disability combined in the world [1]. Upper extremity hemiparesis is one of the most common post-stroke disabilities [2], which negatively affects the activities of daily living and significantly lowers the quality of life [3]. However, the rehabilitation training for patients with upper limb hemiparesis is not easy, which requires long-term professional intensive training. The long-term intensive training not only results in an economic burden on patients and their families but also brings a significant challenge to therapists [4]. Based on the above problems, upper limb exoskeleton rehabilitation devices with the ability to perform repetitive and high-precision tasks and provide assistive force have received more and more attention [5].

Surface electromyography (sEMG) is a noninvasive technique for recording muscle electrical activity, which has been proven to have good performance for human intention recognition [6]. The sEMG-based intention control can be an optimal way to achieve harmonic interactions between subjects and the upper limb rehabilitation exoskeleton. The sEMG-based natural control provides an interface that directly reflects the motion intention of subjects, which is an intuitive actuation method. It can be said that the application of sEMG signals as the control signal is almost tailor-made for rehabilitation exoskeletons. Also, for upper limb exoskeleton systems controlled by sEMG, the accurate identification of the elbow angles from sEMG is essential. There are two kinds of approaches for sEMG-based continuous joint motion estimation: the model-based method and the model-free method [7]. The neuromusculoskeletal modeling combines with muscle physiology, a joint dynamics model with sEMG signal as input is established, and then, the joint torque or angular acceleration is calculated [8]. However, the established model has a complex structure and involves many physiological parameters, which cannot be directly measured, making it difficult for practical applications. Therefore, some researchers consider replacing the biomechanical modeling method with model-free machine learning methods, which is exactly the angle estimation method adopted in this article.

However, there exists subject-specific nature for sEMG signals, which causes the amplitude and frequency to be highly variable among different subjects. As a result, the estimation model with sEMG signals as input has poor generalization across different subjects. To reduce the error from individual differences, Yang et al. [9] built models for each subject, which greatly limits the model generality among multiple subjects, and the workload involved in this method is also too large.

Manuscript received 21 July 2022; revised 1 November 2022; accepted 16 November 2022. Date of publication 28 November 2022; date of current version 12 January 2023. This work was supported in part by the National Natural Science Foundation of China under Grant 61703305, in part by the National High-Tech Research and Development Program (863 Program) of China under Grant 2015AA043202, and in part by SPS KAKENHI under Grant 15K2120. The Associate Editor coordinating the review process was Dr. Priya Ranjan Muduli. *(Corresponding author: Shuxiang Guo.)*

This work involved human subjects or animals in its research. Approval of all ethical and experimental procedures and protocols was granted by the Institutional Review Board (IRB) in the Faculty of Engineering, Kagawa University, (under Ref. No. 01-011 from February 2020), and performed in line with the Declaration of Helsinki.

The authors are with the School of Life Science, Beijing Institute of Technology, Beijing 100081, China, and also with the Key Laboratory of Convergence Biomedical Engineering System and Healthcare Technology, Ministry of Industry and Information Technology, Beijing Institute of Technology, Beijing 100081, China (e-mail: lihe@bit.edu.cn; guoshuxiang@bit.edu.cn).

Digital Object Identifier 10.1109/TIM.2022.3225015

Considering that the high intersubject variability limits the applicability of sEMG in shared control schemes, Trigili et al. [10] performed the selection of a subject-independent feature set of sEMG with the help of information theory tools. To improve the gesture recognition accuracy without training the machine learning algorithm subject specifically, Wahid et al. [11] normalized the time-domain sEMG features to the area under the averaged root-mean-square (rms) curve. He et al. [12] proposed a cross-subject emotion recognition approach from electrocardiogram signals via unsupervised domain adaptation (DA) to train a classifier on a shared subspace with a lower intersubject discrepancy. Bu et al. [13] proposed a subject-independent gesture recognition method based on a transferred learning model. The above methods still only use traditional time- and frequency-domain features, without fundamentally solving the low generalization ability of models caused by intersubject variability. Guo et al. [14] proposed a novel deep multisource DA (MDA) approach, which leverages the information from multiple labeled training subjects to improve the classification performance of the test subject. However, this method is aimed at classification, the deep learning computation is large and the portability is poor. In summary, to the best of our knowledge, this article combines MDA and shallow neural network for the first time to solve the low generalization ability of the neural network model caused by intersubject variability on sEMG, thereby achieving the accurate subject-independent estimation of elbow joint continuous movements.

In this article, based on the consideration of intersubject variability, sEMG-based MDA is adopted to realize the accurate subject-independent estimation of continuous joint movements. In general, time- and frequency-domain features vary among subjects, making the estimation task of sEMG signals challenging. Certainly, the variation in sEMG among multiple subjects creates differences in the data distribution. Through MDA, domain-invariant features can be extracted, in which the sEMG data of a subject represent a domain, data from multiple subjects in the training set constitute the multiple source domains, and the data of the test subject constitute the target domain. The subject-invariant features are then used as the input of the backpropagation neural network (BPNN) to estimate the continuous angle of elbow joints. Furthermore, quantitative analysis is performed by the evaluation criteria, and a statistical analysis is performed through the Bland–Altman (B&A) plot. The experimental results demonstrate that the model established with the subject-invariant features has a better estimation performance, which shows the effectiveness of the combination of MDA and shallow neural network for estimating subject-independent continuous movements of elbow joints accurately.

The rest of this article is organized as follows. In Section II, the experimental protocol is described. In Section III, the methods are illustrated in detail, which mainly includes signal processing, evaluation of feature distribution, MDA, BPNN modeling for sEMG-based angle estimation, calculation of time delay, and evaluation criteria. In Section IV, the results and discussion of the study are reported. Finally, the conclusion is presented in Section V.

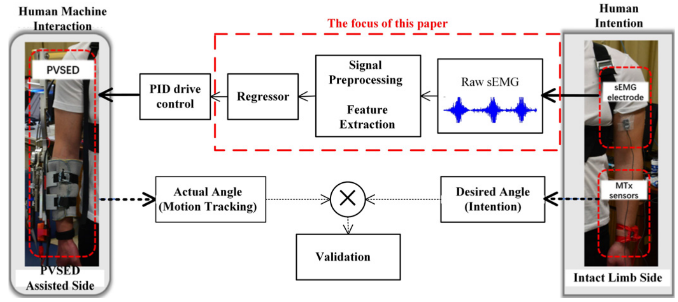


Fig. 1. Human–exoskeleton interaction based on joint angle estimation from sEMG signals [9].

## II. Materials and Methods

### A. System Overview

*1) Research Basic:* Bilateral upper limb rehabilitation training is a rehabilitation training strategy in which the intact side drives the affected side to perform synchronous movements. In a previous study by our research group, a cable-driven powered variable-stiffness exoskeleton device is developed, which was introduced in [15] in detail. Then, an intention-based online bilateral training system for upper limb motor rehabilitation was further proposed [9]. The human–exoskeleton interaction mode using sEMG signals to estimate joint angles is shown in Fig. 1. The sEMG signals during continuous elbow movement are collected in real time. After signal preprocessing and feature extraction, the features are input into the trained regression models to estimate elbow joint angles. The estimation results are used to control the upper limb exoskeleton worn on the affected limb. As a result, the exoskeleton assists the upper limb to perform the desired movements according to the motion intention of subjects. However, it has not been considered from the perspective of intersubject variability to achieve the purpose of improving the accuracy of continuous angle prediction. Therefore, intersubject variability is further considered in this article to realize the subject-independent estimation of continuous joint movements.

*2) Overall Framework of Signal Processing:* The sEMG data are directly streamed to the workspace of MATLAB (MATLAB 2020b, MathWorks) through Bluetooth low energy (BLE) wireless communication and then further processed in MATLAB. The flowchart is shown in Fig. 2, which mainly includes sEMG signal processing, evaluation of feature distribution, MDA, BPNN modeling for sEMG-based angle estimation, calculation of time lag, and the evaluation criteria.

### B. Experimental Protocol

*1) Participants:* In this study, six healthy participants (three males and three females, 22–25 years old) without any history of neuromuscular disorder are chosen. All participants are represented with A–F and the information of the participants is listed in Table I. Before the experiment, each participant is introduced to the experimental protocol and signed the informed consent. All the experimental procedures are

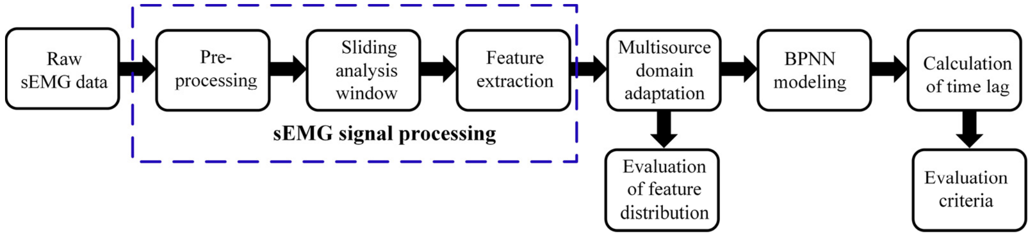


Fig. 2. Flowchart of the processing procedure.

TABLE I
INFORMATION OF SUBJECTS

| Subjects | Gender | Age |
|---|---|---|
| A | male | 25 |
| B | male | 24 |
| C | male | 23 |
| D | female | 25 |
| E | female | 22 |
| F | female | 24 |

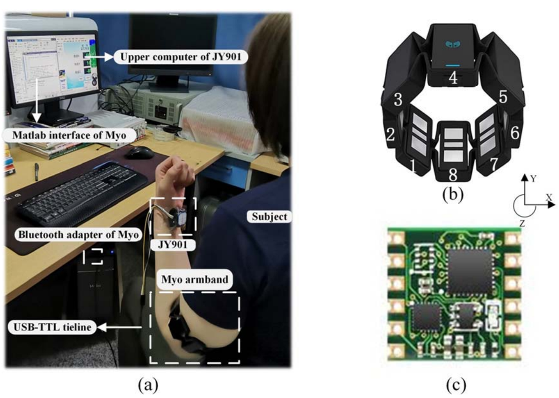


Fig. 3. Experimental setup: (a) schematic of the experimental data acquisition, (b) labeled channels of Myo armband, and (c) IMU.

approved by the Institutional Review Board (IRB) in the Faculty of Engineering, Kagawa University, (Ref. No. 01-011 from February 2020), which follows the ethical principle of Declaration of Helsinki.

*2) Experimental Setup:* The schematic of experimental data acquisition is shown in Fig. 3(a). sEMG signals are obtained using the Myo armband (Thalmic Labs Inc.), which is a commercially available device that includes eight equidistance sEMG sensors. The configuration of Myo armband electrodes is shown in Fig. 3(b), in which the electrode with the LED light and Myo logo that shows the sync state is channel 4, followed by channel 5 in the clockwise direction and channel 3 in the counterclockwise direction. The sEMG data from Myo armband are transmitted to the computer through BLE wireless connection. The real-time sEMG data at a frequency of 200 Hz can be acquired through the software development kit (SDK) of Myo. An inertial measurement unit (IMU) [JY901, WIT motion, Shenzhen, China, as shown in Fig. 3(c)] is also attached to the human forearm to measure the elbow joint movements and used as a reference to verify the estimations, and the sampling frequency of the angle sensor is set to 20 Hz. All the results of the sEMG-based estimations are compared with the measurements of IMU.

*3) Data Acquisition:* Before sEMG signal acquisition, the participants are told to be relaxed to avoid muscle tension, which could introduce offsets to the signal. Meanwhile, the wrist joint and shoulder joint are kept still to avoid the influence of other degree-of-freedom (DOF) movements on the collected sEMG signals, which should only correspond to the single-DOF movements of elbow joints. Myo armband is worn at the same location of each subject's upper arm with channel 4 in the line of the middle finger. After wearing the armband, each participant needs to perform a synchronous gesture to establish a firm connection between the muscle and the armband. When a firm connection has been established, the participant will feel the vibration of Myo armband, and the Myo logo will remain lit instead of flashing; then, the sEMG signal acquisition can be performed. During the sEMG signal acquisition, the forearm should start from the natural drooping state, move around the elbow joint, and return to the natural drooping state after 1 min of movements. Each subject repeats the experiment procedure 5× with 2-min rest between two adjacent experiments to avoid muscle fatigue.

### *C. sEMG Signal Processing*

*1) Preprocessing:* Raw sEMG is the signal generated by muscles, which is very tiny and sensitive to noise. The noise of power-line interference (50 Hz) can be fixed by applying a notch filter to the signal, which will remove the frequency of 50 Hz. Because a 50-Hz notch filter is embedded in Myo armband, there is no need for additional notch filtering. Also, the acquired sEMG data have been normalized to $[-1\ 1]$ through Myo SDK. To remove direct current offsets and the noises in the low-frequency range, a high-pass filter at 20 Hz (fourth-order Butterworth) is applied to the signal. The IMU fuses the nine-axis data (three-axis accelerations, three-axis angular velocities, and three-axis magnetic fields) to calculate quaternion, and furthermore, three-axis Euler angles can be calculated from quaternion. The model also adopts the dynamic Kalman filter algorithm, so the noise of the Euler angle signal output by the IMU is less. Therefore, the angle signals of IMU are not filtered in this article.

*2) Sliding Analysis Window:* Since sEMG signals are highly nonstationary, the most common approach for the processing of sEMG signals is the sliding window approach. The fixed-size overlapping sliding window method is used, which facilitates the introduction of more samples but also helps to reduce the decoding delay in online joint angle estimation [16]. The same technique has been applied to the angle signals obtained from IMU. Due to the real-time characteristics of human–robot interfaces (HRIs), the total time of segment length and processing time of generating estimation control commands should not exceed 300 ms [17]. Therefore, the window length of sEMG is set to 250 ms (50 sample points) with an increment of 50 ms (200 ms overlapping). Also, to make sure that sampling points of sEMG signals are consistent with that of the elbow joint angles obtained by IMU, the IMU angles are also divided into separate windows with a time length of 25 ms (five sample points) and an increment of 5 ms (20-ms overlapping)

*3) Feature Extraction:* Furthermore, to estimate the angle of joint movements, different features should be extracted from each separate window to construct a feature vector [18]. Thus far, features of the time domain (TD), frequency domain (FD), and time–frequency domain (TFD) have been widely used for sEMG signal processing [19]. TD features are closely associated with the amplitude of sEMG, which reflects the angle information. Therefore, the TD features of sEMG perform better on the joint angle estimation than FD and TFD features [20]. Based on the above consideration, three common TD features are extracted from each analysis window in each channel of sEMG signals, which are integrated absolute value (IAV), mean absolute value (MAV), and rms. Based on the number of Myo armband channels and the number of TD features, a 24-dimensional feature vector is constructed.

1) IAV represents the sum of the absolute values of signal amplitude in a separate analysis window, which is defined as

$$\mathrm{IAV} = \sum_{k=1}^{N} |x_k| \tag{1}$$

where $N$ is the number of samples in a separate analysis window and $x_k$ represents the $k$th sample within an analysis window.

2) MAV is evaluated by taking the average of each signal within an analysis window, which is defined as

$$\mathrm{MAV} = \frac{1}{N}\sum_{k=1}^{N} |x_k|. \tag{2}$$

3) RMS refers to the effective value of muscle discharge within an analysis window, and its change depends on the change of sEMG amplitude, which is defined as

$$\mathrm{RMS} = \sqrt{\frac{1}{N}\sum\nolimits_{k=1}^{N} x_k^2}. \tag{3}$$

### *D. Evaluation of Feature Distribution*

sEMG signals have a subject-specific nature, causing the amplitude and spectrum to be variable among different individuals, that is, the intersubject variability [21], [22]. Meanwhile, sEMG signals are time-varying due to their nonstationary nature, which may cause differences when the same subject repeats the same task multiple times, that is, the intrasubject variability [23]. The intersubject and the intrasubject variability are further reflected in the TD feature. Here, kernel density estimation (KDE), which is a nonparametric way to estimate the probability density function of a random variable, is adopted to evaluate the feature distribution corresponding to the following: 1) intersubject variability and 2) intrasubject variability.

Considering one-dimensional data, there are $n$ sample data as follows: $x_1, x_2, x_3, \ldots, x_i, \ldots, x_n$, which have unknown density $f$ at any given point $x$. We are concerned with estimating the shape of this function $f$. The following equation shows the kernel density estimator

$$f(x) = \frac{1}{nh}\sum_{i=1}^{n} K\left(\frac{x - x_i}{h}\right) \tag{4}$$

where $K$ is the kernel and $h$ ($>0$) is the bandwidth, which is a smoothing parameter.

For the evaluation of intrasubject variability, KDE is adopted to calculate the density of MAV features corresponding to the same subject who repeats the same task multiple times, as shown in Fig. 4. Also, for the evaluation of intersubject variability, KDE is adopted to calculate the density of MAV features corresponding to different subjects with the same motion pattern, as shown in Fig. 4. Fig. 5 shows the KDE for the evaluation of intersubject variability. Through Figs. 4 and 5, it can be concluded that intrasubject variability in the continuous movements of the elbow joint is far less pronounced than intersubject variability. Therefore, intersubject variability is the main consideration of this article.

### *E. sEMG-Based MDA*

In machine learning algorithms, the collected data are generally divided into the training set and test set. It is assumed that the training set and the test set conform to the independent and identical distribution, so as to ensure that the model that performs well on the training set is also suitable for the test set. However, in practical problems, the distribution of the test data is often quite different from that of the training data, so the training model cannot have a good prediction effect on the test set. One effective approach to solving the above problem is DA, which can reduce the interdomain discrepancy in the feature level, that is, to learn domain-invariant feature representation. Representative DA algorithms include transfer component analysis (TCA) [24], geodesic flow kernel (GFK) method [25], and maximum independence DA (MIDA) [26].

Due to the high intersubject variability of sEMG, there also exists high different distribution between the training set and the test set, and KDE is adopted to verify it. Therefore, for sEMG data among multiple subjects, traditional machine learning algorithms may not be effective because the assumption of the independent and identical distribution is violated. In our study, the sEMG data of a subject represents a domain, data from multiple subjects in the training set constitute the multiple source domains, and the data of the test subject constitute the target domain. Since more than one source domain is involved, MDA is required instead of single-source DA.

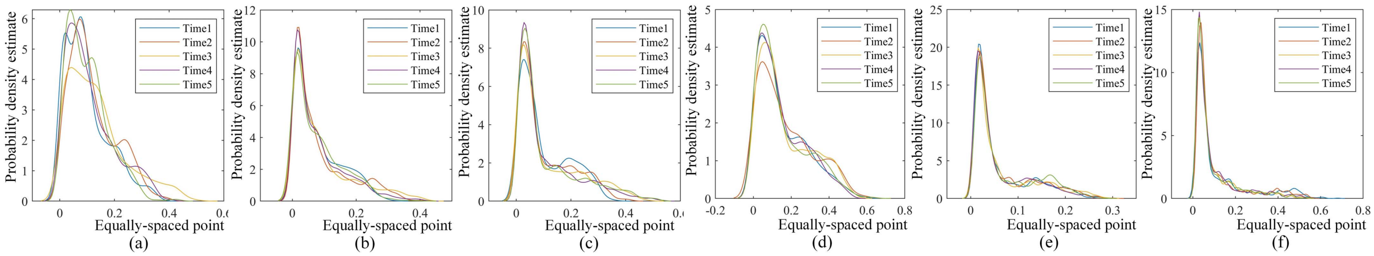


Fig. 4. KDE for the evaluation of intrasubject variability. (a)–(f) KDE corresponding to the subjects A–F, respectively.

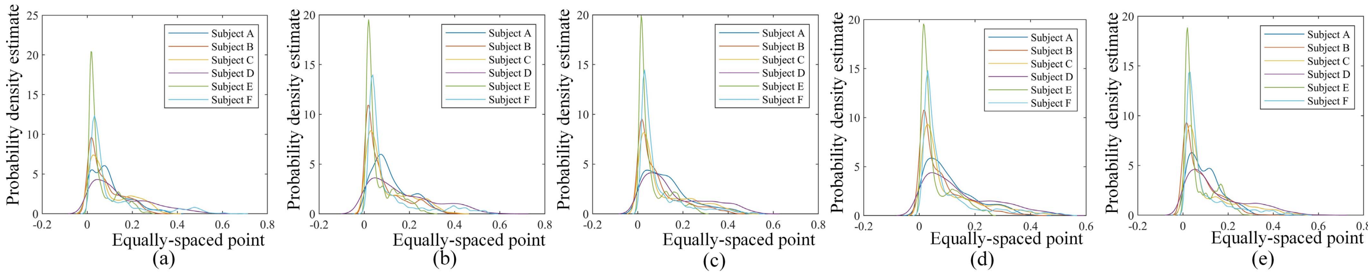


Fig. 5. KDE for the evaluation of intersubject variability. (a)–(e) KDE corresponding to the five measurements, respectively.

Single-source DA involves only one source domain and one target domain, while MDA involves multiple source domains and one target domain, which can collect data from multiple source domains with different distributions. Therefore, the MIDA method that can act as multisource domains is adopted in this article, while TCA and GFK are not suitable to solve the problem in this article.

MIDA is a feature-level MDA algorithm. With the design of domain features, MIDA can be applied to the kind of DA problem with multiple domains. Domain features indicate the background of samples, which represent the subject label in this article. MIDA learns a subspace that is maximally independent of domain features, thereby reducing interdomain discrepancy in distributions. The outline of MIDA is summarized in Algorithm 1.

**Algorithm 1** MIDA

**Input**: The matrix of all samples and their background information; the labels of samples in the source domain; the parameters of kernel function

**Output**: The projected samples.

1. Construct the domain features according to the background information.
2. Augment the original features with domain features.
3. Compute the kernel matrices.
4. Obtain the eigenvectors.
5. The output is the multiplication of the transpose of the projection matrix and the kernel matrix.

### *F. BPNN Modeling for sEMG-Based Angle Estimation*

BPNN is one of the most common and popular techniques used in supervised machine learning, which imitates human neuron activation and transmission process. BPNN is a shallow neural network, its implementation is simple, and the results obtained in practical applications are efficient. The network consists of three layers: the input layer, the hidden layer, and the output layer, where the hidden layer transmits important information between the input layer and the output layer. The process of BPNN is mainly divided into: 1) signal forward propagation and 2) error backpropagation. The BPNN architecture used in this study is given in Fig. 6.

The subject-invariant features extracted through MIDA serve as the input of the input layer of BPNN. The number of nodes in the input and hidden layer both depends on the dimension of a feature vector. The number of input-layer nodes is consistent with the dimension of the feature vector. According to the Kolmogorov superposition theorem, the number of hidden-layer nodes should be equal to $2n + 2$, where $n$ is the number of input-layer nodes. Through the neural network, the estimated angles of elbow motion can be calculated. However, the obtained angle curve is not smooth, so it is filtered using the sliding window method. After sliding window filtering, a smooth angle sequence can be obtained, which can be further applied to HRIs with sEMG as the control signal.

### *G. Calculation of Time Lag*

The IMU used in this article is composed of several sensors, including gyroscopes, accelerometers, and magnetometers. These sensors provide information about the movement after it has been executed, while sEMG signals predict movement intention through machine learning algorithms. Therefore, there is a certain time lag between the angles recorded by the IMU and the angles predicted by sEMG. The time lag between the two kinds of angles is calculated, and the evaluation criteria of mean angle error (MAE) and correlation coefficient (CC) are calculated using the signal after eliminating the time lag. Here, a fast linear correlation (FLC) algorithm is adopted in

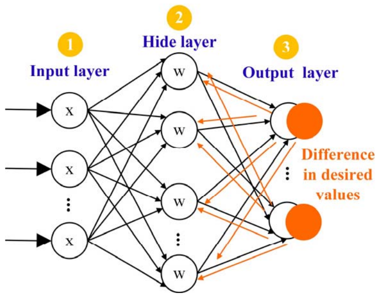


Fig. 6. Schematic of BPNN algorithm.

this article, which is implemented with the help of *xcorr* function in MATLAB. The FLC and cyclic correlation algorithm are common methods that are usually used to calculate the time delay of two sequences, whereas the cyclic correlation algorithm is only applicable to calculating the time delay of aperiodic signals. Although the continuous movements of the elbow joint are not periodic, it has a certain periodic trend, so the FLC algorithm is more suitable for the time lag calculation involved in this article. The outline of FLC algorithm is summarized in Algorithm 2.

**Algorithm 2** FLC

1. Inputs: angle recorded by the IMU ($x(n)$) and angle predicted by sEMG ($y(n)$)
2. Calculate linear correlation with the *xcorr* function
3. Discrete Fourier transformation of $x(n)$ and $y(n)$ is calculated by fast Fourier transform algorithm to obtain X($k$) and Y($k$)
4. Cross-correlation calculation of X($k$) and Y($k$)
5. Make appropriate corrections to the results to get the correlation sequence

### *H. Evaluation Criteria*

The criteria of mean square error (MSE) and regression value (R) are adopted to evaluate the training model performance and additional test performance. Besides the two criteria, MAE and B&A statistical analysis are used to evaluate the estimation performance. MSE is the most common loss function in regression, which represents the mean of the sum of squares of the differences between the predicted angles and the angles, as shown in (5). Also, the larger the MSE value, the closer the predicted angles and the target angles are. MAE is the average error between the predicted angles and the target angles, as shown in (6). CC is used to measure the degree of linear correlation between the predicted angles and the target angles, as shown in (7). The B&A plot is used to compare the consistency between two kinds of measurement data, and the two measurement data in this article correspond to the estimated angle data and the target angle data recorded through IMU. The B&A plot method uses the mean values of two metrics as $x$-axis and the difference between the two metrics as $y$-axis, and then, the scatter distribution within the 1.96 standard deviation line is compared

$$\mathrm{MSE} = \sum_{i=1}^{N} (y_i - x_i)^2 \tag{5}$$

$$\mathrm{MAE} = \frac{1}{N} \sum_{i=1}^{N} (y_i - x_i) \tag{6}$$

$$\mathrm{CC} = \frac{\sum_{i=1}^{N} (x_i - \bar{x})(y_i - \bar{y})}{\sqrt{\sum_{i=1}^{N} (x_i - \bar{x})^2 (y_i - \bar{y})^2}} \tag{7}$$

where $x_i$ represents the actual joint angle at the $i$th data point, $\bar{x}$ is the average value of the actual joint angles of all data points, $\bar{y}$ is the average value of the estimated joint angles of all data points, $y_i$ represents the estimated angle at the $i$th data point, and $N$ is the total number of data points.

## III. Results and Discussion

In this section, the model obtained through BPNN is presented and discussed. To verify the effectiveness of the combination of MDA and the shallow neural network BPNN, the comparisons of feature distribution of training and test set, as well as modeling and prediction effect are provided. Different evaluation indicators are adopted for quantitative evaluation, and the B&A plot is also used for statistical analysis.

### *A. Feature Distribution of Training and Test Sets*

Because of the intersubject variability, the features of sEMG signals of different subjects are different. From Fig. 4, it can be seen that the distribution of sEMG signal features corresponding to different subjects is extremely inconsistent, which verifies the existence of the high intersubject variability. The intersubject variability results in the different distributions of the training set and test set. The training set consists of five subjects, and the test set is one new subject who does not belong to these five subjects. Fig. 7(a) clearly shows the different distributions of the training set and the test set before MIDA. Fig. 7(b) shows the distribution of the training set and the test set after MIDA, from which it can be seen that the distributions of the two are closer after MIDA than that before MIDA, though not exactly the same.

### *B. Regression Model*

The leave-one-subject-out test method is adopted in this study, that is, subjects A–F serve as the test set in turn. Although the specific values of the KDE and evaluation indicators will change with the different test sets, the conclusions are consistent. Therefore, the following analysis is carried out using subject F as an additional test as an example, and subjects A–E are used for modeling. For all subjects (A–F), the data of the first five (A–E) are used for modeling, and the last one (F) serves as the additional test. Samples are randomly divided into the training set, validation set, and test set, the ratio that are 70%:15%:15%, respectively. The training regression value, validation regression value, and test

TABLE II
MODELING PERFORMANCE OF BPNN

| | Training | | Validation | | Test | |
|---|---|---|---|---|---|---|
| | R | MSE | R | MSE | R | MSE |
| Before MIDA | 0.9776 | 113.3496 | 0.9717 | 141.9059 | 0.9709 | 141.4172 |
| After MIDA | 0.9315 | 334.5053 | 0.9301 | 347.4794 | 0.9317 | 336.0335 |

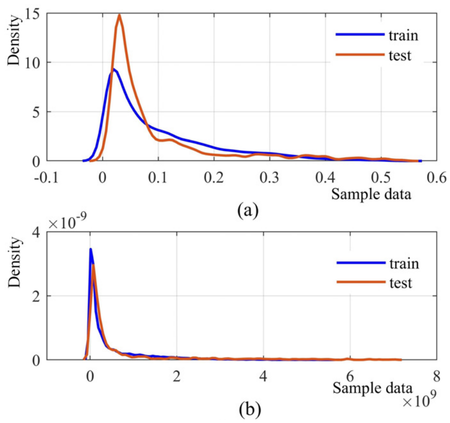


Fig. 7. KDE of the training set and test set (a) before MIDA and (b) after MIDA.

regression value are recorded during the training process. As can be seen from Table I, the regression value (R) and MSE after MIDA are worse than that before MIDA, regardless of training data, verification data, or test data (the larger the R, the better the modeling effect, and the smaller the MSE, the better the modeling effect), which shows that the modeling performance of subject-invariant features is inferior to that of original features. The above phenomenon is due to the reduction of feature dimension after MIDA, the original TD feature dimension is 24, and only two features are retained after MIDA.

## C. Estimation Performance

In the above section, the BPNN models built with the data of the first five subjects (A–E) have been established. In this section, the estimation comparison of the additional test (subject F) will be illustrated. The MSE and R of an additional test are used as the indicator of the angle estimation evaluation, as recorded in Table II. The value of MSE dropped from 1684.6915 before MIDA to 858.2756 after MIDA, R increased from 0.6597 before MIDA to 0.8305 after MIDA, MAE before eliminating the time lag dropped from 26.3123 before MIDA to 20.8587 after MIDA, MAE after eliminating the time lag dropped from 17.9214 before MIDA to 9.7588 after MIDA, CC before eliminating the time lag rises from 0.7870 before MIDA to 0.8720 after MIDA, and CC after eliminating the time lag dropped from 0.8741 before MIDA to 0.9825 after MIDA. In addition, the smaller the MSE and MAE, the better the prediction effect, the larger the R and CC, the better the prediction effect. As can be seen from Table II, the prediction effect of the model built with the subject-invariant features is far better than the model built with the original TD features.

By comparing the results in Tables I and II, it can be seen that although the model established by original features performs well in the source domain, its performance in the target domain is extremely poor, while the model established by subject-invariant features performs poorly in the source domain, but its performance in the target domain is greatly improved compared with the model built with original TD features. The reason why the model established by the original TD feature performs well in the source domain but extremely poorly in the target domain is due to the low generalization ability of the model across multiple subjects. Furthermore, the reason for the low generalization ability of the model is that the TD features are not subject-invariant due to intersubject variability. Through MDA, subject-invariant features can be extracted, which can lead to better generalization ability of the model.

As shown in Table IV, the comparison results of different methods are summarized. Through Table IV, it can be seen that the RMSE of this work is smaller than the original RMSE and also smaller than the RMSE corresponding to the method proposed by Xiao et al. [27]. At the same time, the CC of this work is larger than the original CC and larger than the CC of the method proposed by Xiao et al. [27] and the method proposed by Yang et al. [9]. The method proposed by Yang et al. [9] built a model for each subject, while the method proposed in this article conducts cross-subject research. Therefore, it is acceptable even if the RMSE of the method proposed by Yang et al. [9] is slightly smaller than the corresponding RMSE of our method, and the gap is not large.

As can be seen from Fig. 8(a) and (c), the angles recorded by IMU are not completely synchronized with the angles estimated by the neural network model, and there exists a certain time lag. The time lag is calculated through FLC, and the result is shown in Fig. 8(e), through which it can be known that there are nine points of phase error in the two signal sequences. Since the window length of sEMG is set to 250 ms with an increment of 50 ms, the time lag between the two signals is 450 ms ($9 \times 50 = 450$ ms). Reasons for the angles predicted by sEMG to be ahead of the angles recorded by IMU include the following: 1) sEMG is generally generated 30–150 ms ahead of limb movements and 2) sliding windowing makes the current signals have the trend of future signals.

The B&A plots of estimated and actual angles are shown in Fig. 9, each containing 1196 observations of subject F. It can

TABLE III
ESTIMATION COMPARISON OF THE ADDITIONAL TEST BEFORE AND AFTER MIDA

| | MSE | R | MAE | | CC | |
|---|---|---|---|---|---|---|
| | | | With time lag | Without time lag | With time lag | Without time lag |
| Before MIDA | 1684.6915 | 0.6597 | 26.3123 | 17.9214 | 0.7870 | 0.8741 |
| After MIDA | 858.2756 | 0.8305 | 20.8587 | 9.7588 | 0.8720 | 0.9825 |

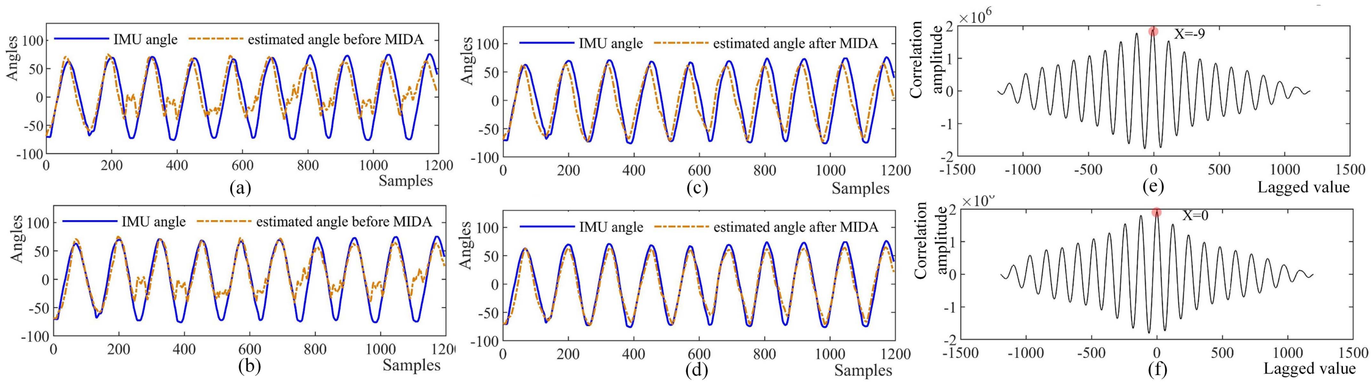


Fig. 8. Estimated angles and time lag (a) angle estimation through the model built with TD features—before time lag elimination, (b) angle estimation through the model built with TD features—after time lag elimination, (c) angle estimation through the model built with subject-invariant features—before time lag elimination, (d) angle estimation through the model built with subject-invariant features—after time lag elimination, (e) phase difference between the estimated angles and IMU angles before time lag elimination, and (f) phase difference between the estimated angles and IMU angles after time lag elimination.

TABLE IV
COMPARISON OF PREDICTION PERFORMANCE WITH OTHER METHODS

| | sEMG Channel Number | Features | Results | |
|---|---|---|---|---|
| | | | RMSE | CC |
| Initial data | 8 | 3 | 0.57 | 0.8741 |
| Yang [9] | 2 | 9 | 0.16 | 0.8940 |
| Xiao [27] | 2 | 5 | 0.39 | 0.9228 |
| This paper | 8 | 3 | **0.27** | **0.9825** |

be seen from Fig. 9 that the data distribution after MIDA is more centralized than that before MIDA. The absolute value of the "Mean" value with a time lag after MIDA (value = 2.9) is far less than that before MIDA (value = −9.5), as shown in Fig. 8(a) and (c). The absolute value of the "Mean" value without time lag after MIDA adaptation (value = 3.5) is far less than that before MIDA (value = −8.9), as shown in Fig. 8(b) and (d). The above shows that the prediction results of the model built with the subject-invariant features are closer to the actual angle (i.e., IMU angle) than the model built with the original TD features. From the comparison of Fig. 8(a) and (c) [or Fig. 8(b) and (d)], it can be known that the existence of time lag between the estimated angles and IMU angles, and the two kinds of angles after eliminating the time lag are closer.

As shown in Table V, the comparison with the state of the art is recorded. Yang et al. [9], Trigili et al. [10], and Guo et al. [14] all considered intersubject variability and adopted different ideas to solve it. Yang et al. [9] used common TD features and FD features to build models for each subject. Trigili et al. [10] selected subject-independent features with the help of the information theory tool. However, these features are only a subset of the initial traditional features. To sum up, Yang et al. [9] and Trigili et al. [10] still only use traditional time- and frequency-domain features, without fundamentally solving the low generalization ability of models caused by intersubject variability. Guo et al. [14] leveraged deep learning to overcome individual differences in challenging abnormal gait detection, this article focuses on recognition accuracy. The methods of Yang et al. [9] and Trigili et al. [10] can be used in the online application, and the method of Guo et al. [14] is for offline mode.

In our article, subject-invariant features are obtained through MDA. Compared with the method of Guo et al. [14], the method in this article has the potential to be applied to real-time applications due to the simplicity of the network model involved. However, the current processing flows are performed offline, but how to apply the research framework in this study to the online stage to control the exoskeleton device in real time is still a difficult problem. As far as I know, the existing online MDA method has a relatively serious delay and cannot meet the requirements of HRIs. To the best of our knowledge,

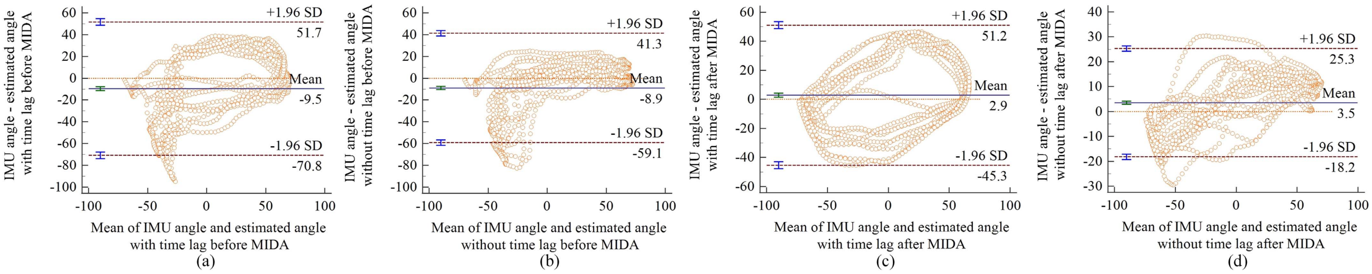


Fig. 9. B&A plots of the IMU angles and estimated angles (a) with time lag before MIDA, (b) without time lag before MIDA, (c) with time lag after MIDA, and (d) without time lag after MIDA.

TABLE V
COMPARISON WITH THE STATE OF THE ART

| | Control mode | Feature type | Prediction type |
|---|---|---|---|
| Yang [9] | Online | TD/FD/TFD features | Regression |
| Trigili [10] | Online | TD/FD/TFD features | Regression |
| Guo [14] | Offline | Subject-invariant features | Classification |
| This paper | **Offline** | **Subject-invariant features** | **Regression** |

there is no relevant literature that applies MDA to the upper limb rehabilitation exoskeleton system. Therefore, one key of our future research direction is the online DA method that can be applied to real-time HRIs.

Besides the study of the online DA method, intrasubject variability also needs to be further considered. Although intersubject variability has a greater impact on the generalization ability of the model, intrasubject variability cannot be ignored. The intersubject variability is caused by the nonstationarity of sEMG, which varies time, leading to intrasubject variability that may also reduce the generalization ability of the model. Therefore, our research group will also dedicate to studying the method, which can reduce intrasubject discrepancy, thus taking both the intersubject variability and intrasubject variability into account.

## IV. CONCLUSION

In this article, the MDA and a shallow neural network BPNN are combined to solve the problem of intersubject variability on sEMG during the continuous movements of elbow joints. In the processing of MDA, each subject is seen as a domain to extract domain-invariant (i.e., subject-invariant) features. Furthermore, BPNN is adopted to estimate the angles by using the subject-invariant features. The experiment result shows that the model built with subject-invariant features has better generalization ability among multiple subjects, compared with that built with original TD features. In the future, the study on the online MDA will be further considered, which can be used in the real-time control of upper limb exoskeleton rehabilitation devices. Also, both intersubject variability and intrasubject variability will also be considered into account.

## ACKNOWLEDGMENT

The authors would like to acknowledge all the subjects for participating in this study.

## REFERENCES

[1] V. L. Feigin et al., "World stroke organization (WSO): Global stroke fact sheet 2022," *Int. J. Stroke.*, vol. 17, no. 1, pp. 18–29, 2022, doi: 10.1177/17474930211065917.

[2] C. Ersoy and G. Iyigun, "Boxing training in patients with stroke causes improvement of upper extremity, balance, and cognitive functions but should it be applied as virtual or real?" *Topics Stroke Rehabil.*, vol. 28, no. 2, pp. 112–126, Feb. 2021, doi: 10.1080/10749357.2020.1783918.

[3] Q. Meng et al., "Pilot study of a powered exoskeleton for upper limb rehabilitation based on the wheelchair," *BioMed. Res. Int.*, vol. 2019, Dec. 2019, Art. no. 9627438, doi: 10.1155/2019/9627438.

[4] J. Narayan, B. Kalita, and S. K. Dwivedy, "Development of robot-based upper limb devices for rehabilitation purposes: A systematic review," *Augmented Hum. Res.*, vol. 6, no. 1, pp. 1–33, Dec. 2021, doi: 10.1007/s41133-020-00043-x.

[5] J. M. Veerbeek, A. C. Langbroek-Amersfoort, E. E. H. Van Wegen, C. G. M. Meskers, and G. Kwakkel, "Effects of robot-assisted therapy for the upper limb after stroke," *Neurorehabilitation Neural Repair*, vol. 31, no. 2, pp. 107–121, Feb. 2017, doi: 10.1177/1545968316666957.

[6] Y. Zhang, Y. Chen, H. Yu, X. Yang, and W. Lu, "Learning effective Spatial–Temporal features for sEMG armband-based gesture recognition," *IEEE Internet Things J.*, vol. 7, no. 8, pp. 6979–6992, Aug. 2020, doi: 10.1109/jiot.2020.2979328.

[7] L. Bi, A. G. Feleke, and C. Guan, "A review on EMG-based motor intention prediction of continuous human upper limb motion for human-robot collaboration," *Biomed. Signal Process. Control*, vol. 51, pp. 113–127, May 2019, doi: 10.1016/j.bspc.2019.02.011.

[8] Y. Zhao, Z. Zhang, Z. Li, Z. Yang, A. A. Dehghani-Sanij, and S. Xie, "An EMG-driven musculoskeletal model for estimating continuous wrist motion," *IEEE Trans. Neural Syst. Rehabil. Eng.*, vol. 28, no. 12, pp. 3113–3120, Dec. 2020, doi: 10.1109/TNSRE.2020.3038051.

[9] Z. Yang, S. Guo, Y. Liu, H. Hirata, and T. Tamiya, "An intention-based online bilateral training system for upper limb motor rehabilitation," *Microsyst. Technol.*, vol. 27, no. 1, pp. 211–222, Jan. 2021, doi: 10.1007/s00542-020-04939-x.

[10] E. Trigili et al., "Detection of movement onset using EMG signals for upper-limb exoskeletons in reaching tasks," *J. Neuroeng. Rehabil.*, vol. 16, no. 1, p. 45, 2019, doi: 10.1186/s12984-019-0512-1.

[11] M. F. Wahid, R. Tafreshi, M. Al-Sowaidi, and R. Langari, "Subject-independent hand gesture recognition using normalization and machine learning algorithms," *J. Comput. Sci.*, vol. 27, pp. 69–76, Jul. 2018, doi: 10.1016/j.jocs.2018.04.019.

[12] W. He, Y. Ye, Y. Li, T. Pan, and L. Lu, "Online cross-subject emotion recognition from ECG via unsupervised domain adaptation," in *Proc. 43rd Annu. Int. Conf. IEEE Eng. Med. Biol. Soc. (EMBC)*, Nov. 2021, pp. 1001–1005.

[13] D. Bu, S. Guo, and H. Li, "SEMG-based motion recognition of upper limb rehabilitation using the improved YOLO-v4 algorithm," *Life*, vol. 12, no. 1, p. 64, Jan. 2022, doi: 10.3390/life12010064.

[14] Y. Guo, X. Gu, and G.-Z. Yang, "MCDCD: Multi-source unsupervised domain adaptation for abnormal human gait detection," *IEEE J. Biomed. Health Informat.*, vol. 25, no. 10, pp. 4017–4028, Oct. 2021, doi: 10.1109/JBHI.2021.3080502.

[15] Y. Liu, S. Guo, Z. Yang, H. Hirata, and T. Tamiya, "A home-based bilateral rehabilitation system with sEMG-based real-time variable stiffness," *IEEE J. Biomed. Health Informat.*, vol. 25, no. 5, pp. 1529–1541, May 2021, doi: 10.1109/JBHI.2020.3027303.

[16] J. Liu, Y. Ren, D. Xu, S. H. Kang, and L.-Q. Zhang, "EMG-based real-time linear-nonlinear cascade regression decoding of shoulder, elbow, and wrist movements in able-bodied persons and stroke survivors," *IEEE Trans. Biomed. Eng.*, vol. 67, no. 5, pp. 1272–1281, May 2020, doi: 10.1109/TBME.2019.2935182.

[17] K. Li, J. Zhang, L. Wang, M. Zhang, J. Li, and S. Bao, "A review of the key technologies for sEMG-based human-robot interaction systems," *Biomed. Signal Process. Control*, vol. 62, Sep. 2020, Art. no. 102074, doi: 10.1016/j.bspc.2020.102074.

[18] J. Kim, B. Koo, Y. Nam, and Y. Kim, "SEMG-based hand posture recognition considering electrode shift, feature vectors, and posture groups," *Sensors*, vol. 21, no. 22, p. 7681, Nov. 2021, doi: 10.3390/s21227681.

[19] P. Angkoon, N. K. Rami, and S. J. S. Erik, "Feature extraction and selection for myoelectric control based on wearable EMG sensors," *Sensors*, vol. 18, no. 5, pp. 1651–1667, 2018, doi: 10.3390/s18051615.

[20] X. Xi et al., "Simultaneous and continuous estimation of joint angles based on surface electromyography state-space model," *IEEE Sensors J.*, vol. 21, no. 6, pp. 8089–8099, Jan. 2021, doi: 10.1109/jsen.2020.3048983.

[21] T. Bao, S. A. R. Zaidi, S. Xie, P. Yang, and Z.-Q. Zhang, "Inter-subject domain adaptation for CNN-based wrist kinematics estimation using sEMG," *IEEE Trans. Neural Syst. Rehabil. Eng.*, vol. 29, pp. 1068–1078, 2021, doi: 10.1109/TNSRE.2021.3086401.

[22] K. Zhao, Z. Zhang, H. Wen, and A. Scano, "Intra-subject and inter-subject movement variability quantified with muscle synergies in upper-limb reaching movements," *Biomimetics*, vol. 6, no. 4, p. 63, Oct. 2021, doi: 10.3390/biomimetics6040063.

[23] D. Rimini, V. Agostini, and M. Knaflitz, "Intra-subject consistency during locomotion: Similarity in shared and subject-specific muscle synergies," *Front. Hum. Neurosci.*, vol. 11, p. 586, Dec. 2017, doi: 10.3389/fnhum.2017.00586.

[24] S. J. Pan, I. W. Tsang, J. T. Kwok, and Q. Yang, "Domain adaptation via transfer component analysis," *IEEE Trans. Neural Netw.*, vol. 22, no. 2, pp. 199–210, Feb. 2011, doi: 10.1109/TNN.2010.2091281.

[25] B. Gong, S. Yuan, S. Fei, and K. Grauman, "Geodesic flow kernel for unsupervised domain adaptation," in *Proc. IEEE Conf. Comput. Vis. Pattern Recognit.*, Jun. 2012, pp. 2066–2073. [Online]. Available: https://ieeexplore.ieee.org/document/6247911.

[26] K. Yan, L. Kou, and D. Zhang, "Learning domain-invariant subspace using domain features and independence maximization," *IEEE Trans. Cybern.*, vol. 48, no. 1, pp. 288–299, Jan. 2018, doi: 10.1109/TCYB.2016.2633306.

[27] F. Xiao, Y. Wang, Y. Gao, Y. Zhu, and J. Zhao, "Continuous estimation of joint angle from electromyography using multiple time-delayed features and random forests," *Biomed. Signal Process. Control*, vol. 39, pp. 303–311, Jan. 2018, doi: 10.1016/j.bspc.2017.08.015.


**He Li** (Student Member, IEEE) received the M.S. degree from the School of Precision Instrument and Opto-Electronics Engineering, Tianjin University, Tianjin, China, in 2021. She is currently pursuing the Ph.D. degree with the Beijing Institute of Technology, Beijing, China.

She has published five refereed journal and conference papers. Her research interests include exoskeleton rehabilitation robots, sEMG signal processing, and telerehabilitation systems.

**Shuxiang Guo** (Fellow, IEEE) received the Ph.D. degree in mechanoinformatics and systems from Nagoya University, Nagoya, Japan, in 1995.

He is currently the Chair Professor with the Beijing Institute of Technology, Beijing, China. His current research interests include biomimetic underwater robots, minimal invasive surgery robot systems, and rehabilitation robotics.

Dr. Guo is an Editor-in-Chief of the International Journal of Mechatronics and Automation.

**Hanze Wang** (Student Member, IEEE) received the B.S. degree from the School of Biomedical Engineering, Beijing Institute of Technology, Beijing, China, in 2021, where he is currently pursuing the M.S. degree.

He has published one conference papers. His research interests include exoskeleton rehabilitation robotic systems for biomedical applications.

**Dongdong Bu** (Student Member, IEEE) received the M.S. degree in electronics and communication engineering from the Beijing Institute of Technology, Beijing, China, in 2017, where he is currently pursuing the Ph.D. degree.

He has published two refereed journals and conference papers. His research interests include exoskeleton rehabilitation robotic systems for biomedical applications.